Prediction of obstructive coronary artery disease using coronary calcification and epicardial adipose tissue assessments from CT calcium scoring scans

Prediction of obstructive coronary artery disease using coronary calcification and epicardial adipose tissue assessments from CT calcium scoring scans

Juhwan Lee, Tao Hu, Michelle C Williams, Ammar Hoori, Hao Wu, Justin N Kim, David E Newby, Robert Gilkeson, Sanjay Rajagopalan, David L Wilson

Abstract

Background

Low-cost/no-cost non-contrast CT calcium scoring (CTCS) exams can provide direct evidence of coronary atherosclerosis. In this study, using features from CTCS images, we developed a novel machine learning model to predict obstructive coronary artery disease (CAD), as defined by the coronary artery disease-reporting and data system (CAD-RADS).

Methods

This study analyzed 1324 patients from the SCOT-HEART trial who underwent both CTCS and CT angiography. Obstructive CAD was defined as CAD-RADS 4A-5, while CAD-RADS 0–3 were considered non-obstructive CAD. We analyzed clinical, Agatston-score-derived, and epicardial fat-omics features to predict obstructive CAD. The most predictive features were selected using elastic net logistic regression and used to train a CatBoost model. Model performance was evaluated using 1000 repeated five-fold cross-validation and survival analyses to predict major adverse cardiovascular event (MACE) and revascularization. Generalizability was assessed using an external validation set of 2316 patients for survival predictions.

Results

Among the 1324 patients, obstructive CAD was identified in 334 patients (25.2 %). Elastic net regression identified the top 14 features (5 clinical, 2 Agatston-score-derived, and 7 fat-omics). The proposed method achieved excellent performance for classifying obstructive CAD, with an AUC of 90.1 ± 0.9 % and sensitivity/specificity/accuracy of 83.5 ± 5.5 %/93.7 ±

1.9 %/82.4 ± 2.0 %. The inclusion of Agatston-score-derived and fat-omics features significantly improved classification performance. Survival analyses showed that both actual and predicted obstructive CAD significantly differentiated patients who experienced MACE and revascularization.

Conclusions

We developed a novel machine learning model to predict obstructive CAD from non-contrast CTCS scans. Our findings highlight the potential clinical benefits of CTCS imaging in identifying patients likely to benefit from advanced imaging.

1 Introduction

Obstructive coronary artery disease (CAD) remains a leading cause of death worldwide, accounting for 17.8 million deaths annually,(1, 2) highlighting the need for advanced diagnostic tools to predict and mitigate its progression. Early and accurate prediction of CAD is essential for timely intervention and improved patient outcomes. Among various imaging modalities, coronary computed tomography angiography (CCTA) is considered the most reliable for assessing the presence and severity of obstructive CAD, offering detailed insights into coronary artery conditions.

CCTA provides a clear, detailed view of the coronary arteries, making it indispensable for diagnosing and managing CAD. The coronary artery disease reporting and data system (CAD-RADS) standardizes CCTA reporting and categorizes CAD severity, ranging from CAD-RADS 0 (no plaque or stenosis) to CAD-RADS 5 (100 % occlusion), with additional categories for patients with previous interventions. (3) CAD-RADS has been reported as a strong predictor of major adverse cardiovascular events (MACE) in numerous studies. (4-9) However, its use is limited by cost, the need for contrast agents, and ionizing radiation exposure. Additionally, predicting clinical outcomes based solely on CCTA can be challenging, particularly in cases with mild or ambiguous findings.

Non-contrast CT calcium scoring (CTCS) directly detects coronary atherosclerosis when calcifications are present and is recognized by several guidelines as a preferred risk assessment tool. (10, 11) However, no studies have assessed whether CTCS can predict obstructive CAD. While CTCS is well-established for cardiovascular risk assessment, its potential for identifying obstructive disease remains unexplored. We hypothesize that quantitative coronary measurements from CTCS are related to obstructive CAD. Specifically,

we identified CTCS-derived features associated with obstructive CAD, as defined by CCTA CAD-RADS. This analysis not only highlights key CTCS features linked to obstructive disease but also enables further correlation with CCTA to identify high-risk plaque features. In this regard, we developed novel hand-crafted feature sets using CTCS (i.e., calcium-omics (12) and fat-omics (13)), which were strongly associated with future MACE outcomes. Given CTCS's unique ability to assess coronary plaque, relating its findings to cardiovascular risk evaluated by CCTA presents a compelling opportunity.

In this study, we developed a novel machine learning model to predict obstructive CAD from CTCS scans and evaluated its predictive performance using extensive multi-center datasets. We incorporated various clinical features, Agatston score-derived features, and epicardial fat-omics features (13) and determined the most relevant features. Then, we trained multiple machine learning models and compared their predictive performance for obstructive CAD.

2 Methods

2.1 Study population

This study was a sub-study of the Scottish COmputed Tomography of the HEART (SCOT-HEART) multicenter randomized controlled trial (NCT01149590). The main study was approved by the local ethics committee, and written informed consent was provided by all participants. This sub-study was approved and conducted under the data use agreement between the University of Edinburgh, Edinburgh, UK, and the University Hospitals Cleveland Medical Center, Cleveland, Ohio, USA. The primary results have been published previously. (14-16) In brief, of the 4146 trial participants who attended the cardiology outpatient clinic, 2073 were randomized to the intervention arm. Of these, 1778 underwent CT, and 1324 scans were available and of suitable quality for analysis in this study. More details are provided in elsewhere. (17, 18)

2.2 CT imaging

All participants underwent both non-contrast electrocardiogram-gated CTCS and contrast enhanced electrocardiogram-gated CCTA (Figure 1). Imaging was performed using either 64- or 320-detector row scanners (Brilliance 64, Philips Medical Systems, Netherlands; Biograph mCT, Siemens, Germany; Aquilion ONE, Toshiba Medical Systems, Japan). Tube current, voltage, and volume of iodine-based contrast were adjusted based on body mass index.

2.3 CAD-RADS assessment

CAD-RADS assessment of all CCTA scans was performed using standardized semi-automatic software (AutoPlaque, Version 2.5, Cedars-Sinai Medical Center, Los Angeles, California, USA). The CAD-RADS classification was divided into six categories according to the highest

grade of coronary stenosis detected in any vessel (3): CAD-RADS 0 (0 % stenosis: documented absence of CAD), CAD-RADS 1 (1–24 % stenosis: minimal non-obstructive CAD), CAD-RADS 2 (25–49 % stenosis: mild non-obstructive CAD), CAD-RADS 3 (50–69 % stenosis: moderate stenosis), CAD-RADS 4A (70–99 % stenosis: severe stenosis), CAD-RADS 4B (>50 % stenosis in left main or ≥70 % stenosis in three vessels), and CAD-RADS 5 (100 % stenosis: total occlusion). In our study, obstructive CAD was defined as CAD-RADS 4A-5, and CAD-RADS 0–3 were considered non-obstructive CAD.

2.4 Feature extraction

We analyzed 29 clinical, 6 Agatston score-derived, and 211 fat-omics features to predict the obstructive CAD. 1) The clinical features included baseline characteristics (e.g., age, gender, and body mass index), blood tests results (e.g., cholesterol level), and medication prescriptions (e.g., statin, ACE inhibitor, and beta-blockers). Chest pain was categorized into two groups – cardiac chest pain and non-cardiac chest pain – according to current guidelines. (19, 20) Table 1 shows the clinical features analyzed as predictors of obstructive CAD. 2) The Agatston score-derived features encompassed the Agatston scores of all coronary arteries (i.e., left anterior descending (LAD), left circumflex artery (LCX), right coronary artery (RCA), left main (LM), and total), logarithms of the Agatston scores, and the diffusivity index.(21) To prevent the output from being infinity, we added 1 to the Agatston score for the logarithm function (Table 2). The diffusivity index was calculated as a continuous variable by taking the Agatston score of the most affected vessel (the vessel with the highest individual Agatston score), dividing it by the total Agatston score, and then subtracting this value from 1 (equation: 1 – (Agatston score of the most affected vessel/total Agatston score)).(21) A higher diffusivitry index indicates a more diffuse distribution of

coronary artery calcification, while a lower diffusivity index indicates that a larger proportion of the total coronary artery calcification is concentrated in a single artery. 3) We included a total of 211 handcrafted, pathophysiologically-inspired fat-omics features, categorized into three groups: morphological, intensity, and spatial features. (13) To extract these features, we segmented the epicardial adipose tissue regions within the pericardium using our previously developed DeepFat method. (22) Morphological features included measurements such as volume, principal axis lengths, and epicardial fat thickness. Intensity features comprised statistical metrics, including the minimum, maximum, and mean Hounsfield units (HU), skewness, and histogram bins. For spatial analysis of fat distribution within the heart region, we divided the heart area into four equally thick slabs of image slices from top to bottom and four equidistant ribbons from the outer to inner regions. Detailed descriptions of these fat-omics features are provided elsewhere. (13)

2.5 Feature selection

We used elastic net regression,(23) which combines the properties of both Lasso (L1) and Ridge (L2) regularization, to select the best features for the classification models. Specifically, we set the mixing parameter (α) to 0.5 to equally balance the strengths of the L1 and L2 penalties. A sequence of 100 regularization values (λ) was automatically generated on a logarithmic scale, ranging from a maximum value that results in all coefficients being zero to a minimum value. We utilized 5-fold cross-validation to tune these hyperparameters and to prevent overfitting. During this process, the data was split into five subsets, and the model was iteratively trained on four subsets while being validated on the remaining subset. This ensured that the model was robust and generalized well to unseen data. All feature selection and model training were performed on the training set.

2.6 Development of machine learning model

After selecting the best features using Elastic Net regression, we trained a machine learning model using the CatBoost algorithm.(24) CatBoost, a gradient boosting algorithm, is particularly adept at handling categorical variables and mitigating overfitting, making it especially advantageous for medical data classification. To optimize the CatBoost model, we performed hyperparameter tuning using grid search. The hyperparameters tuned included the number of iterations (100), learning rate (0.01), depth (6), L2 leaf regularization (5), random subspace method (0.75), border count (64), loss function (logloss), evaluation metric (F1), bootstrap type (Bernoulli), subsample (0.6), and thread count (1). This grid search allowed us to identify the best combination of hyperparameters for our specific dataset. These hyperparameters were determined using all combined features (model 3 described below).

We developed and trained three different models using various combinations of features: (model 1) clinical features only, (model 2) clinical + Agatston score, and (model 3) all combined. Each model was trained using the same hyperparameter optimization process.

2.7 Performance evaluation

To ensure the robustness and reliability of our model, we utilized 1000 repeated 5-fold cross-validation. This method involved splitting the dataset into five subsets, training the model on four subsets, and validating it on the remaining subset. This process was repeated 1000 times to average out variability and prevent overfitting. The classification performance was

quantitatively assessed using conventional metrics, including sensitivity, specificity, accuracy, and area under the receiver operating characteristic curve (AUC), as shown below:

We reported the mean and standard deviation of all metrics over the five folds.

Furthermore, to investigate performance variance, we compared the performance of the optimized CatBoost model against three other established methods: Support Vector Machine (SVM), (25) Random Forest (RF), (26) and XGBoost. (27) Training details for all machine learning models are provided in Supplementary Table 1. Each model was trained and tested using the same dataset split to ensure a fair comparison. This comprehensive evaluation allowed us to determine the most effective machine learning approach for our classification task.

In addition to conventional metrics, we performed more clinically relevant assessments. Following classification, we used both actual and predicted obstructive CAD to assess the risk of MACE and revascularization through Kaplan-Meier and Cox proportional hazards analyses. MACE was defined as a composite of nonfatal myocardial infarction, nonfatal stroke, cardiovascular death, and revascularization. Revascularization was defined as a composite of coronary artery bypass grafting and percutaneous coronary intervention. Additionally, a subset of the CLARIFY trial (NCT04075162), consisting of 2316 patients who underwent both CCTA and CTCS, served as the external validation set for survival predictions. Please note that these datasets were used only for survival predictions, as CAD-RADS scores were not available.

2.8 Statistical analysis

We evaluated the value of clinical, Agatston score-derived, and fat-omics features as predictors of obstructive CAD using various statistical approaches. Continuous features were

presented as mean ± standard deviation, while categorical features were reported as frequencies. Statistical comparisons between obstructive and non-obstructive CAD groups were performed using a student's t-test for continuous variables and a Chi-square test for categorical variables. For the prediction of MACE, both Kaplan-Meier and Cox proportional hazard analyses were employed, with 95 % confidence intervals (CI) and hazard ratio (HR) calculated. Statistical significance was defined as a p-value less than 0.05. All statistical analyses were performed using R Studio software (version 2024.04.1, R Foundation for Statistical Computing, Vienna, Austria).

3 Results

This study included 1324 patients who underwent both CCTA and CTCS examinations. No patients were excluded based on clinical characteristics or image analysis results. Among the 1324 patients, obstructive CAD was identified in 334 patients (25.2 %). The distribution of patients across CAD-RADS scores was as follows: 0 (472, 35.6 %), 1 (248, 18.7 %), 2 (150, 11.3 %), 3 (120, 9.1 %), 4A (160, 12.1 %), 4B (30, 2.3 %), and 5 (144, 10.9 %). The mean ages between obstructive and non-obstructive CAD groups were 55.9 ± 9.5 years and 61.2 ± 7.7 years respectively ($p < 0.05$). The baseline characteristics of the study population between obstructive and non-obstructive CAD groups are presented in Table 1.

Agatston score-derived features were significantly different between obstructive and non-obstructive CAD groups ($p < 0.05$) (Table 2). Particularly, the logarithmic expression of Agatston scores led to much higher differentiations between the two groups. The diffusivity index was also significantly different between the groups. The total Agatston score was gradually increased as the CAD-RADS score increased from 0 to 5 ($p < 0.05$). The total Agatston scores for each CAD-RADS category were 0: 2.3 ± 28.7, 1: 41.9 ± 64.8, 2: 216.8 ± 308.8, 3: 393.2 ± 532.7.4A: 591.2 ± 878.3, 4B: 957.8 ± 903.0, and 5: 1192.0 ± 1541.0, respectively (Figure 2).

Starting with 247 combined features, including 25 clinical, 11 Agatston score-derived, and 211 fat-omics features, we selected the top 14 features for model 3 using Elastic Net regression.(23) Among these top 14 features, five were clinical features, two were Agatston score features, and seven were fat-omics features (Figure 3). Notably, the top three features were all fat-omics features related to the probability of epicardial fat voxels (SR3_Pro_190_170, SR4_Pro_190_170, and SR4_Pro_170_150) (Supplementary Table S2).

The best features for other models (models 1–2) were also determined by Elastic Net and are shown in Supplementary Figure S1.

Our method (Model 3) achieved excellent classification of obstructive CAD, with an AUC of 90.1 ± 0.9 %, a sensitivity of 83.5 ± 5.5 %, a specificity of 93.7 ± 1.9 %, and an accuracy of 82.4 ± 2.0 %, across folds (Table 3). Model 1 (clinical) showed the lowest performance with a sensitivity of 58.4 %. However, the addition of Agatston score-derived features (Model 2) significantly improved classification performance. Adding fat-omics to existing models further improved sensitivity by 3 %, from 80.5 % to 83.5 % (Model 3), highlighting the importance of fat-omics features. The predictive performances of other models are provided in the Supplementary Table S3. Compared to other established machine learning methods, CatBoost showed the best classification results (Table 4). Although SVM had highest sensitivity, with much smaller standard deviation, its overall specificity was exceptionally low compared to other methods. Both RF and XGBoost methods showed high specificity of >90 %, but their sensitivity was low (<74 %). Other classification results are provided in Supplementary Tables S4–S5.

We assessed the ability of our obstructive CAD classification model for predicting MACE and revascularization. Both the actual and predicted obstructive CAD significantly distinguished between MACE and no-MACE groups ($p < 0.00001$) (Figure 4 A and B), as well as between revascularization and no-revascularization groups in Kaplan-Meier analyses ($p < 0.00001$) (Figure 4 C and D). In the Cox proportional hazard analyses predicting MACE, the HR for predicted CAD was 4.7 (95 % CI: 3.1–7.3; C-index: 0.545; $p < 0.00001$), compared to an HR of 18.6 (95 % CI: 13.1–26.5; C-index: 0.816; $p < 0.00001$) for actual obstructive CAD. For predicting revascularization, the actual and predicted CADs showed similar tendencies (HR: 25.7; 95 % CI: 17.0–39.0; C-index: 0.835, $p < 0.00001$ vs. HR: 5.0; 95 % CI: 3.2–7.7; C-index:

0.548; p < 0.00001). When we applied the proposed method to the external validation set (n = 2316) for survival predictions, our method showed significant discrimination between MACE and no-MACE groups, as well as between revascularization and no-revascularization, with HRs of 2.4 (95 % CI: 2.0–3.1; C-index: 0.600; p < 0.00001) and 9.8 (95 % CI: 4.8–20.0; C-index: 0.759; p < 0.00001), respectively (Figure 5). Please note that predictions using actual obstructive CAD were not provided, as it was not available.

4 Discussion

Building on our previous studies utilizing CTCS imaging (12, 13, 22, 28-33) we developed a novel machine learning model to predict obstructive CAD from CTCS scans and evaluate its clinical value for survival predictions. This study offers several key contributions. First, we incorporated unique feature sets consisting of clinical, Agatston score-derived, and most importantly, epicardial fat-omics features.(13) The most relevant features were determined using elastic net logistic regression. Second, we utilized various state-of-the-art machine learning methods and compared their classification performance with different feature groups. This comprehensive evaluation allowed us to determine the most effective machine learning approach for our purposes. Third, unlike other classification/regression studies, we further investigated the clinical value of our method for predicting MACE and revascularization using extensive multi-center datasets.

A combination of clinical, Agatston score-derived, and fat-omics features showed the best classification results for obstructive CAD. Among the top 14 features, the clinical features included chest pain, diabetes mellitus, hyperlipidemia, coronary heart disease family history, and gender. This finding aligns with many previous studies. (34-38 For example, the CAD Consortium (CAD2) model, a most common clinical prediction tool for estimating obstructive CAD, includes age, sex, chest pain, diabetes mellitus, hypertension, hyperlipidemia, and smoking status. (34) In a landmark study, (35) Al'Aref et al. reported that gender, hyperlipidemia, diabetes mellitus, and chest pain are strongly associated with obstructive CAD, supporting the reliability of our findings. Regarding coronary artery calcification aspects, we found that Agatston score-derived features (i.e., diffusivity index and logarithmic total Agatston score) add value in predicting obstructive CAD, as shown in Table 3. Several studies have correlated the Agatston score with obstructive CAD.(35-39) For instance, Ren

et al.(36) investigated the added value of the Agatston score to traditional cardiovascular risk factors and found that the Agatston score was more important than other variables. These studies support the reliability of our prediction model. Additionally, we found the added advantage of fat-omics for improving classification performance (Table 3). Specifically, the spatial distribution of epicardial fat voxels had the strongest impact among all features. This finding is somewhat different from our previous study.(13) In our previous study,(13) we identified the top 15 fat-omics features to predict MACE using the Cox proportional hazard model with Elastic regularization. Most features were related to epicardial adipose tissue volume and thickness. However, in this study, the fat-omics features were predominantly associated with the probabilities of fat voxels in specific spherical regions.

Our method demonstrated high reproducibility, as assessed by extensive multi-center datasets, including the SCOT-HEART and CLARIFY trials. This multi-center evaluation is crucial because it ensures that the model's performance is robust and generalizable across diverse patient populations and imaging conditions. Although there were small discrepancies in HR and C-index between the training and external validation sets, our method significantly predicted both MACE and revascularization (Figures 4 and 5). By training and testing on datasets from different centers, we mitigated the risk of overfitting to a single-center dataset, which could limit the model's applicability in other settings. Our consistent classification performance across multiple independent cohorts highlights its reliability and potential for broader clinical adoption in predicting obstructive CAD from CTCS data. Such validation is essential for establishing trust in the model's predictions and for ensuring its effectiveness in real-world clinical environments.

The findings of the present study have significant clinical implications. Current interpretation methods for CTCS images, endorsed by European Society of Cardiology, American Heart

Association, and American College of Cardiology, do not assess potential drivers of obstructive CAD. Several attempts have been made to develop and validate machine learning models to predict obstructive CAD using traditional cardiovascular risk factors(35, 39) alongside traditional scoring systems, such as the CAD Consortium 2 (34) and the updated Diamond-Forrester score.(40) Al'Aref et al.(35) developed an XGBoost-based machine learning model using clinical features and Agatston score to predict the presence of obstructive CAD. Similarly, Ren et al. (36) investigated the predictive value of clinical variables combined with Agatston score for predicting obstructive CAD in individuals with atypical chest pain. Wang et al.(38) also combined clinical features with the Agatston score to predict obstructive CAD and compared results using multiple machine learning approaches. Miller et al.(37) suggested simple likelihood tables using the Agatston score and clinical variables (e.g., age, sex, and chest pain) to predict obstructive CAD. Although these studies claim strengths and high predictability, none have incorporated imaging-derived features, indicating room for improvement. For the first time, we have quantitatively analyzed CTCS imaging data, particularly fat-omics, to improve the prediction of obstructive CAD. By predicting obstructive disease from CTCS images, we provide a method to identify patients who would likely benefit from additional advanced imaging (e.g., CCTA), all from low-cost or no-cost screening CTCS exams.

This study has several limitations. First, our focus on obstructive CAD rather than non-obstructive CAD may not fully align with the recent shift in cardiovascular research, which emphasizes non-obstructive CAD as an important entity and target for prevention. Additionally, a recent randomized controlled trial (41) has questioned the benefit of routine revascularization in stable obstructive CAD. Future studies should further investigate the predictive value of fat-omics for non-obstructive CAD. Second, external validation was

performed only for survival predictions due to the absence of CAD-RADS measurements. While our survival prediction was promising and reproducible, the relatively small sample size may affect the reproducibility of obstructive CAD predictions, and outcomes might differ with a larger population. Therefore, further studies using external validation datasets are warranted. Third, although our method provided promising predictions, uncertainty remains regarding the reproducibility and clinical applicability of quantitative CTCS image analysis. Additionally, intra- and inter-operator variability in radiomic evaluation may impact the consistency of feature extraction and model performance. To address this, further studies using repetitive (i.e., scan-to-rescan) CTCS data are warranted to evaluate the reproducibility of our fat-omics features. Fourth, although the fat-omics calculations were fully automated, each CTCS scan assessment took 10–15 min. Future advancements in software automation could facilitate broader application. Finally, incorporating additional quantified variables, such as calcium-omics,(12) could improve predictive performance.

In conclusion, we developed a novel machine learning model to predict obstructive CAD from non-contrast CTCS scans and evaluated its clinical value using extensive multi-center datasets. Our findings highlight the potential clinical benefits of utilizing CTCS imaging to evaluate patients who require further examination (e.g., CCTA) for obstructive CAD.

References

1. Roth GA, Abate D, Abate KH, et al. Global, regional, and national age-sex-speci c mortality for 282 causes of death in 195 countries and territories, 1980–2017: a systematic analysis for the Global Burden of Disease Study 2017. Lancet. 2018; 392(10159):1736–1788. https://doi.org/10.1016/S0140-6736(18)32203-7.
2. Nichols M, Townsend N, Scarborough P, Rayner M. Cardiovascular disease in Europe 2014: epidemiological update. Eur Heart J. 2014;35(42):2950–2959. https://doi.org/10.1093/eurheartj/ehu299.
3. Cury RC, Leipsic J, Abbara S, et al. CAD-RADSTM 2.0– 2022 coronary artery disease–reporting and data system an expert consensus document of the society of cardiovascular computed tomography (SCCT), the American College of cardiology (ACC), the American College of radiology (ACR) and the north America society of cardiovascular imaging (NASCI). Radiology: Cardiothoracic Imaging. 2022;4(5): e220183. https://doi.org/10.1148/ryct.220183.
4. Altay S. Prognostic value of standard coronary computed tomography angiography reporting system (CAD-RADS). Indian J Radiol Imag. 2021;31(1):37–42. https://doi.org/10.1055/s-0041-1729128.
5. Bittner DO, Mayrhofer T, Budoff M, et al. Prognostic value of coronary CTA in stable chest pain: CAD-RADS, CAC, and cardiovascular events in PROMISE. JACC Cardiovasc Imaging. 2020;13(7):1534–1545. https://doi.org/10.1016/j.jcmg.2019.09.012.
6. Lee JW, Kim JY, Han K, et al. Coronary CT angiography CAD-RADS versus coronary artery calcium score in patients with acute chest pain. Radiology. 2021;301(1):81–90. https://doi.org/10.1148/radiol.2021204704.
7. Senoner T, Plank F, Barbieri F, et al. Added value of high-risk plaque criteria by coronary CTA for prediction of long-term outcomes. Atherosclerosis. 2020;300:26–33. https://doi.org/10.1016/j.atherosclerosis.2020.03.019.
8. Tang CX, Qiao HY, Zhang XL, et al. Functional CAD-RADS using FFRCT on therapeutic management and prognosis in patients with coronary artery disease. Eur Radiol. 2022;32(8):5210–5221. https://doi.org/10.1007/s00330-022-08618-5.
9. Williams MC, Moss A, Dweck M, et al. Standardized reporting systems for computed tomography coronary angiography and calcium scoring: a real-world validation of CAD-RADS and CAC-DRS in patients with stable chest pain. J Cardiovasc Comput Tomogr. 2020;14(1):3–11. https://doi.org/10.1016/j.jcct.2019.07.010.
10. Orringer CE, Blaha MJ, Blankstein R, et al. The National Lipid Association scienti c statement on coronary artery calcium scoring to guide preventive strategies for ASCVD risk reduction. Journal of Clinical Lipidology. 2021;15(1):33–60. https://doi.org/10.1016/j.jacl.2020.12.005.
11. Golub IS, Termeie OG, Kristo S, et al. Major global coronary artery calcium guidelines. JACC (J Am Coll Cardiol): Cardiovascular Imaging. 2023;16(1):98–117. https://doi.org/10.1016/j.jcmg.2022.06.018.
12. Hoori A, Al-Kindi S, Hu T, et al. Enhancing cardiovascular risk prediction through AI-enabled calcium-omics. Sci Rep. 2024;14(1):11134. https://doi.org/10.1038/s41598-024-60584-8.
13. Hu T, Freeze J, Singh P, et al. Arti cial intelligence prediction of cardiovascular events using opportunistic epicardial adipose tissue assessments from computed

tomography calcium score. JACC (J Am Coll Cardiol): Adv. 2024;3(9):101188. https://doi.org/10.1016/j.jacadv.2024.101188.
14. Newby DE, Adamson PD, Berry C, et al. Coronary CT angiography and 5-year risk of myocardial infarction. N Engl J Med. 2018;379(10):924–933. https://doi.org/10.1056/NEJMoa1805971.
15. CT coronary angiography in patients with suspected angina due to coronary heart disease (SCOT-HEART): an open-label, parallel-group, multicentre trial. Lancet. 2015; 385(9985):2383–2391. https://doi.org/10.1016/S0140-6736(15)60291-4.
16. Williams MC, Hunter A, Shah ASV, et al. Use of coronary computed tomographic angiography to guide management of patients with coronary disease. J Am Coll Cardiol. 2016;67(15):1759–1768. https://doi.org/10.1016/j.jacc.2016.02.026.
17. Williams MC, Jacek K, Mhairi D, et al. Low-attenuation noncalci ed plaque on coronary computed tomography angiography predicts myocardial infarction. Circulation. 2020;141(18):1452–1462. https://doi.org/10.1161/CIRCULATIONAHA.119.044720.
18. Williams MC, Moss AJ, Dweck M, et al. Coronary artery plaque characteristics associated with adverse outcomes in the SCOT-heart study. J Am Coll Cardiol. 2019; 73(3):291–301. https://doi.org/10.1016/j.jacc.2018.10.066.
19. Gulati M, Levy PD, Mukherjee D, et al. AHA/ACC/ASE/CHEST/SAEM/SCCT/SCMR guideline for the evaluation and diagnosis of chest pain. A Report of the American College of Cardiology/American Heart Association Joint Committee on Clinical Practice Guidelines. Circulation. 2021;144(22):e368–e454. https://doi.org/10.1161/CIR.0000000000001029, 2021.
20. Knuuti J, Wijns W, Saraste A, et al. 2019 ESC Guidelines for the diagnosis and management of chronic coronary syndromes: the Task Force for the diagnosis and management of chronic coronary syndromes of the European Society of Cardiology (ESC). Eur Heart J. 2020;41(3):407–477. https://doi.org/10.1093/eurheartj/ehz425.
21. Blaha MJ, Budoff MJ, Tota-Maharaj R, et al. Improving the coronary artery calcium score– addition of regional measures of calcium distribution: multi-ethnic study of atherosclerosis (MESA). JACC Cardiovasc Imaging. 2016;9(12):1407–1416. https://doi.org/10.1016/j.jcmg.2016.03.001.
22. Hoori A, Hu T, Lee J, Al-Kindi S, Rajagopalan S, Wilson DL. Deep learning segmentation and quanti cation method for assessing epicardial adipose tissue in CT calcium score scans. Sci Rep. 2022;12(1):2276. https://doi.org/10.1038/s41598-022-06351-z.
23. Zou H, Hastie T. Regularization and variable selection via the elastic net. J Roy Stat Soc B. 2005;67(2):301–320. https://doi.org/10.1111/j.1467-9868.2005.00503.x.
24. Prokhorenkova L, Gusev G, Vorobev A, Dorogush AV, Gulin A. CatBoost: unbiased boosting with categorical features. In: Advances in Neural Information Processing Systems. 31. Curran Associates, Inc.; 2018. https://proceedings.neurips.cc/paper_ les/paper/2018/hash /14491b756b3a51daac41c24863285549-Abstract.html. Accessed June 3, 2024.
25. Cortes C, Vapnik V. Support-vector networks. Mach Learn. 1995;20(3):273–297. https://doi.org/10.1007/BF00994018.
26. Ho Tin Kam. Random decision forests. In: Proceedings of 3rd International Conference on Document Analysis and Recognition. 1. IEEE Comput. Soc. Press; 1995:278–282. https://doi.org/10.1109/ICDAR.1995.598994.

27. Chen T, Guestrin C. XGBoost: a scalable tree boosting system. In: Proceedings of the 22nd ACM SIGKDD International Conference on Knowledge Discovery and Data Mining. KDD'16. Association for Computing Machinery; 2016:785–794. https://doi.org/10.1145/2939672.2939785.
28. Song Y, Hoori A, Wu H, et al. Improved bias and reproducibility of coronary artery calci cation features using deconvolution. JMI. 2023;10(1):014002. https://doi.org/10.1117/1.JMI.10.1.014002.
29. Hoori A, Freeze J, Singh P, et al. Prediction of major adverse cardiovascular events using comprehensive AI analysis of calci cations and fat depots in CT calcium score images. In: Gimi BS, Krol A, eds. Medical Imaging 2024: Clinical and Biomedical Imaging. SPIE. 2024:10. https://doi.org/10.1117/12.3003977.
30. Hoori A, Hu T, Lee J, Al-kindi S, Rajagopalan S, Wilson DL. An enriched survival study of epicardial adipose tissues risk on major adverse cardiovascular event in CT calcium score images. In: Gimi BS, Krol A, eds. Medical Imaging 2023: Biomedical Applications in Molecular, Structural, and Functional Imaging. SPIE. 2023:27. https://doi.org/10.1117/12.2653613.
31. Wu H, Song Y, Hoori A, et al. Translating non-contrast CT calcium score images to virtual CCTA to aid segmentation of coronary arteries and myocardium. In: Medical Imaging 2024: Clinical and Biomedical Imaging. 12930. 2024:26–31. https://doi.org/10.1117/12.3006516. SPIE.
32. Hu T, Hoori A, Lee J, et al. AI predictions of major adverse cardiovascular event using epicardial and paracardial adipose tissue assessments in CT calcium score images. In: Gimi BS, Krol A, eds. Medical Imaging 2024: Clinical and Biomedical Imaging. SPIE. 2024:11. https://doi.org/10.1117/12.3006789.
33. Song Y, Wu H, Lee J, et al. Pericoronary Adipose Tissue Feature Analysis in CT Calcium Score Images with Comparison to Coronary CTA. 2024. https://doi.org/10.48550/arXiv.2401.15554. Published online January 27.
34 Genders TSS, Steyerberg EW, Hunink MGM, et al. Prediction model to estimate presence of coronary artery disease: retrospective pooled analysis of existing cohorts. BMJ. 2012;344:e3485. https://doi.org/10.1136/bmj.e3485.
35. Al'Aref SJ, Maliakal G, Singh G, et al. Machine learning of clinical variables and coronary artery calcium scoring for the prediction of obstructive coronary artery disease on coronary computed tomography angiography: analysis from the CONFIRM registry. Eur Heart J. 2020;41(3):359–367. https://doi.org/10.1093/eurheartj/ehz565.
36. Ren Y, Li Y, Pan W, Yin D, Du J. Predictive value of CAC score combined with clinical features for obstructive coronary heart disease on coronary computed tomography angiography: a machine learning method. BMC Cardiovasc Disord. 2022;22(1):569. https://doi.org/10.1186/s12872-022-03022-9.
37. Miller RJH, Gransar H, Rozanski A, et al. Simpli ed approach to predicting obstructive coronary disease with integration of coronary calcium: development and external validation. J Am Heart Assoc. 2023;12(24):e031601. https://doi.org/10.1161/JAHA.123.031601.
38. Wang M, Sun M, Yu Y, Li X, Ren Y, Yin D. Predictive value of machine learning algorithm of coronary artery calcium score and clinical factors for obstructive coronary artery disease in hypertensive patients. BMC Med Inf Decis Making. 2023;23(1):244. https://doi.org/10.1186/s12911-023-02352-8.

39. Hu J, Hao G, Xu J, Wang X, Chen M. Deep learning-based coronary artery calcium score to predict coronary artery disease in type 2 diabetes mellitus. Heliyon. 2024; 10(6):e27937. https://doi.org/10.1016/j.heliyon.2024.e27937.
40. Fihn SD, Gardin JM, Abrams J, et al. 2012 ACCF/AHA/ACP/AATS/PCNA/SCAI/STS guideline for the diagnosis and management of patients with stable ischemic heart disease: a report of the American College of cardiology foundation/American heart association task force on practice guidelines, and the American College of physicians, American association for thoracic surgery, preventive cardiovascular nurses association, society for cardiovascular angiography and interventions, and society of thoracic surgeons. Circulation. 2012;126(25):e354–e471. https://doi.org/10.1161/CIR.0b013e318277d6a0.
41. Maron DJ, Hochman JS, Reynolds HR, et al. Initial invasive or conservative strategy for stable coronary disease. N Engl J Med. 2020;382(15):1395–1407. https://doi.org/10.1056/NEJMoa1915922.

Figures

Figure 1 A representative example of paired CTCS and CCTA images showing three diseased vessels. The CAD-RADS was 4B, and the total Agatston score was 2089 (LAD: 1,316, LCX: 492, and RCA: 281).

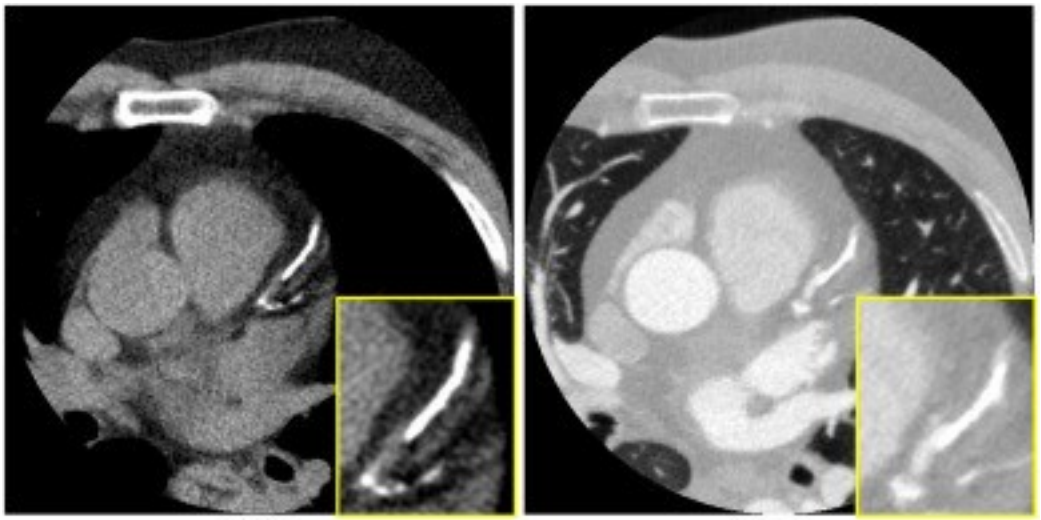

Figure 2 Correlations between CAD-RADS and total Agatston score. The total Agatston scores for each CAD-RADS category were 0: 2.3 ± 28.7, 1: 41.9 ± 64.8, 2: 216.8 ± 308.8, 3: 393.2 ± 532.7, 4A: 591.2 ± 878.3, 4B: 957.8 ± 903.0, and 5: 1192.0 ± 1541.0, respectively.

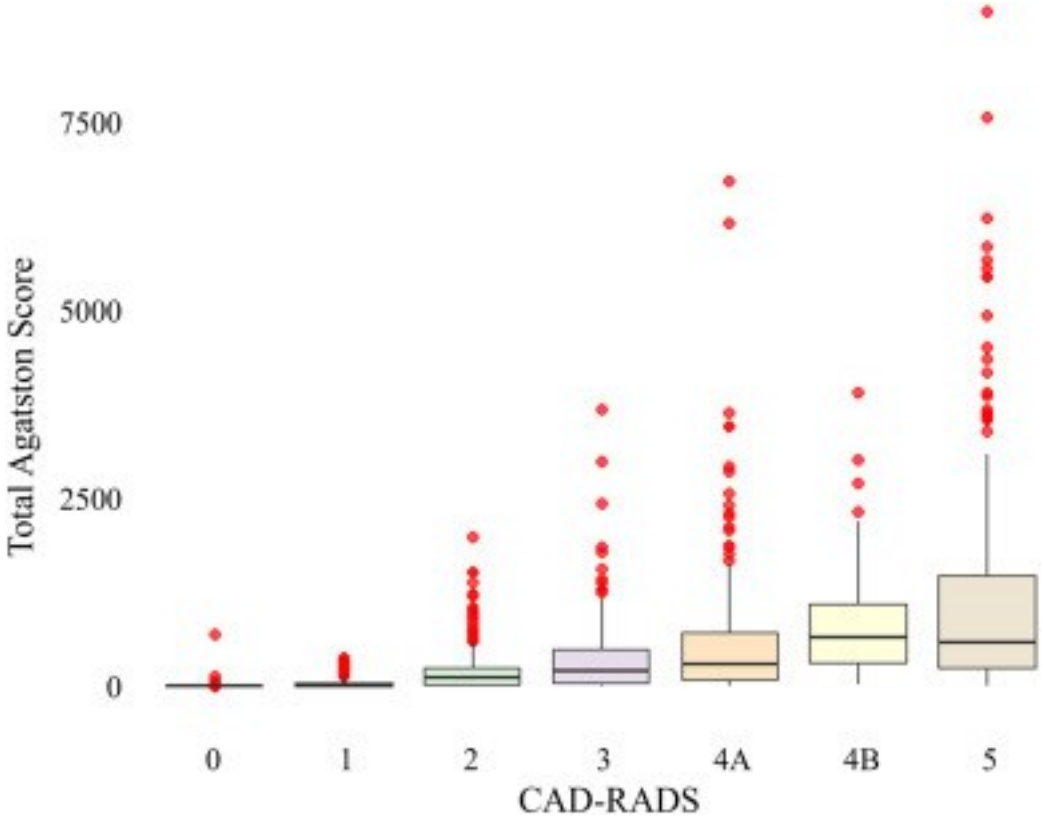

Figure 3 Variable importance plot of the top 14 features (model 3) selected by Elastic Net regression. The top 14 features included five clinical features, two Agatston score-derived features, and seven fat-omics features. The 95 % confidence interval is provided for each feature.

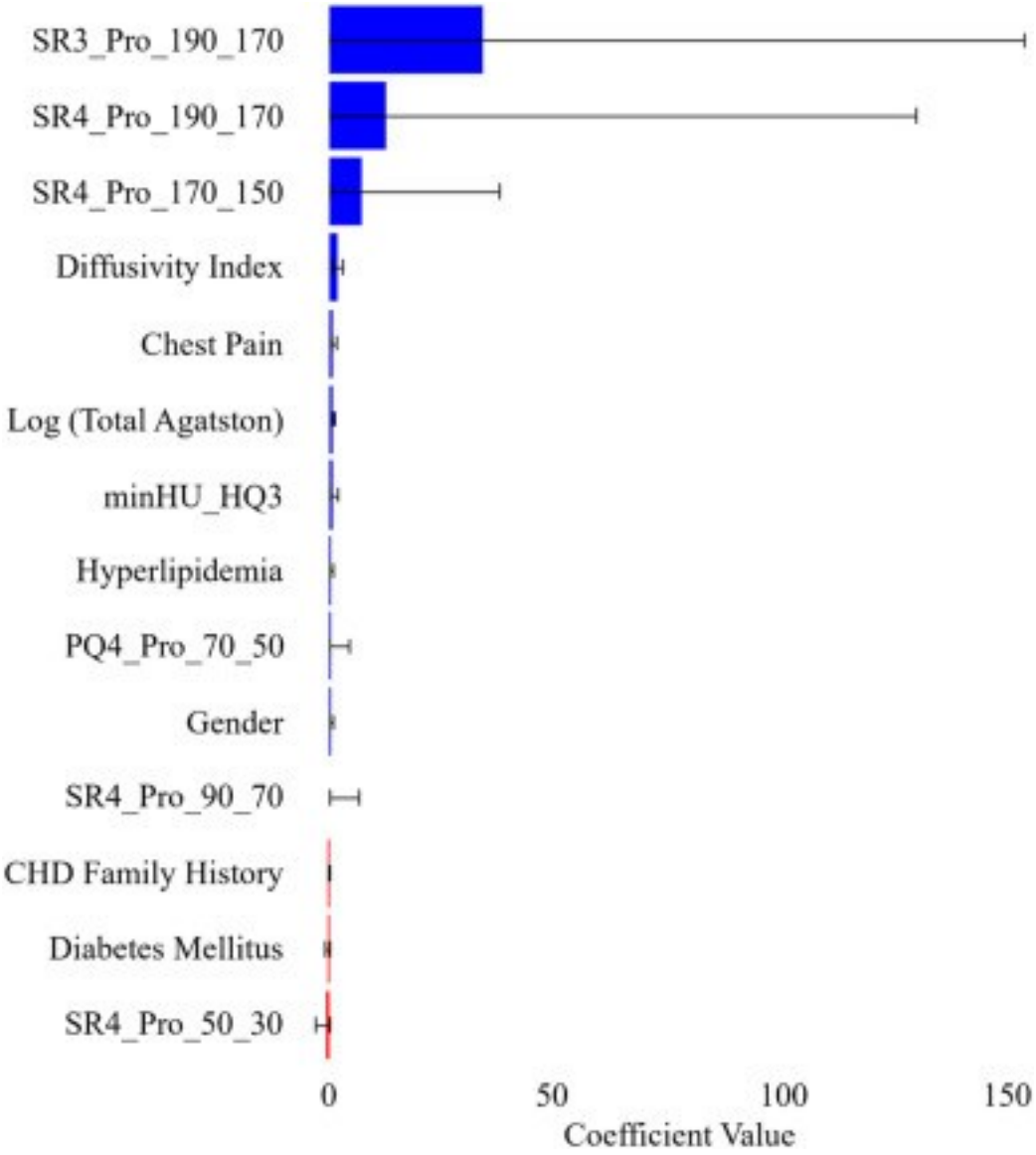

Figure 4 Kaplan-Meier survival curves for MACE (A: actual CAD and B: predicted CAD) and revascularization (C: actual CAD and D: predicted CAD) obtained using five-fold cross-validation. The x-axis represents survival time, and the y-axis represents the survival probability of patients. Both the actual and predicted obstructive CAD significantly differentiated between the MACE and no-MACE groups ($p < 0.00001$), as well as between the revascularization and no-revascularization groups ($p < 0.00001$).

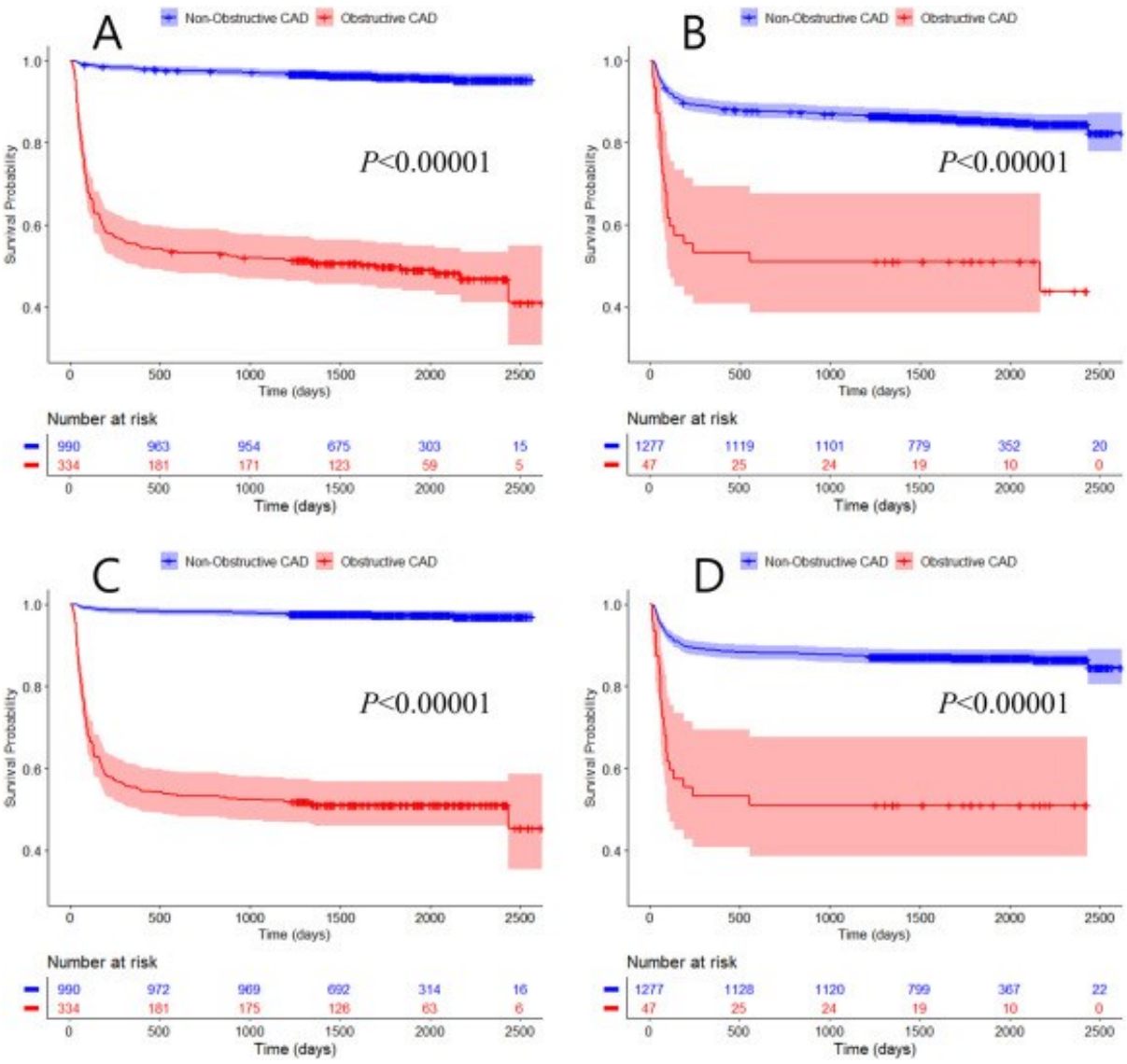

Figure. 5 Kaplan-Meier survival curves for MACE (A) and revascularization (B) on the external validation set consisting of 2316 patients. For survival analysis, the CatBoost model was trained using the entire SCOT-HEART data (n = 1324) and applied to the external validation set. The output of the trained model was used for survival analysis. The x-axis represents survival time, and the y-axis represents the survival probability of patients. Our method significantly differentiated between the MACE and no-MACE groups ($p < 0.00001$), as well as between the revascularization and no-revascularization groups ($p < 0.00001$).

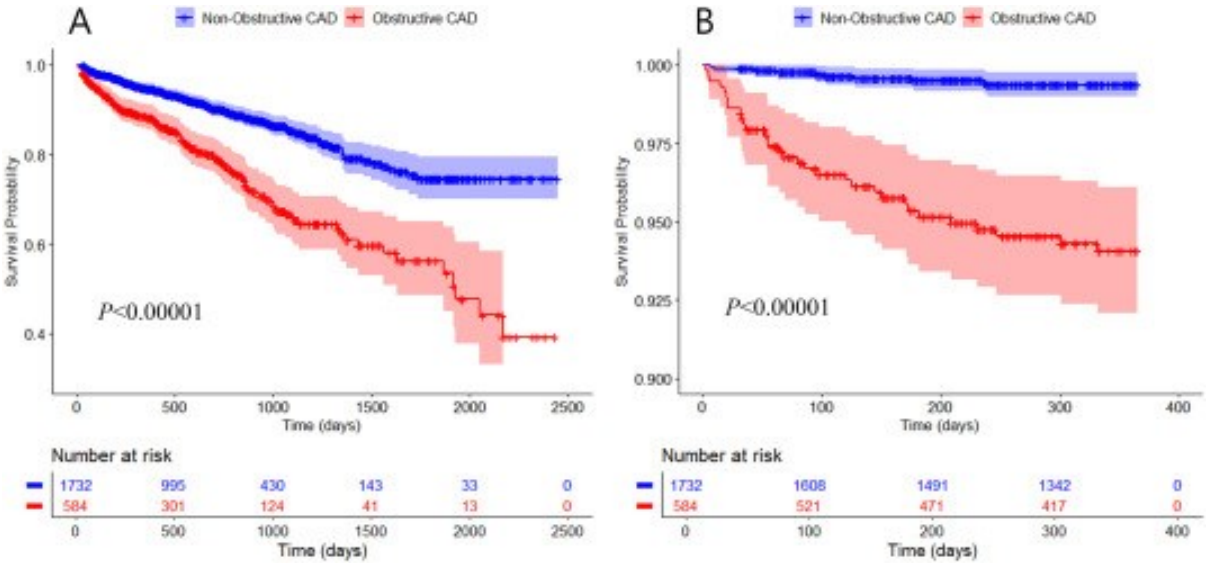

Tables

Table 1

Baseline clinical characteristics of obstructive and non-obstructive CAD groups (BMI: body mass index, HDL: high-density lipoprotein, and CHD: congenital heart disease).

Features	Total (n = 1324)	Obstructive (n = 334)	Non-obstructive (n = 990)	p-value
Male	737/1324 (55.7 %)	254/334 (76.0 %)	483/990 (48.8 %)	0.418
BMI	29.6 ± 5.6	29.4 ± 4.8	29.7 ± 5.8	0.513
Age	57.3 ± 9.4	61.2 ± 7.7	55.9 ± 9.5	<0.001
BMI band (≥30 or <30)	534/1324	132/334 (39.5 %)	402/990 (40.6 %)	0.515
Age band (18–59 or 60–75)	577/1324	196/334 (58.7 %)	381/990 (38.5 %)	0.670
Diabetes Mellitus	148/1324	45/334 (13.5 %)	103/990 (10.4 %)	0.875
Height	1.70 ± 0.10	1.72 ± 0.1	1.69 ± 0.10	<0.001
Weight	85.4 ± 17.8	86.7 ± 16.1	84.9 ± 18.3	0.111
Smoking habit[a]	No: 631/1323 (47.7 %) Prior: 441/1323 (33.3 %) Current:	No: 149/334 (44.6 %) Prior: 119/334 (35.6 %)	No: 482/989 (48.7 %) Prior: 322/989 (32.6 %)	0.729

	251/1323 (19.0 %)	Current: 66/334 (19.8 %)	Current: 185/989 (18.7 %)	
Cigarettes per day	2.8 ± 7.1	2.9 ± 6.8	2.8 ± 7.2	0.949
Hypertension	459/1324 (34.7 %)	151/329 (45.9 %)	308/981 (31.4 %)	0.556
Total cholesterol	5.0 ± 1.9	5.1 ± 2.0	5.0 ± 1.8	0.545
HDL cholesterol	1.0 ± 0.7	0.9 ± 0.6	1.1 ± 0.7	<0.05
CHD family history	584/1324 (44.1 %)	143/333 (42.9 %)	441/981 (45.0 %)	0.946
Systolic blood pressure	138.3 ± 24.0	142.2 ± 21.6	137.0 ± 24.6	0.0005
Diastolic Blood Pressure	81.2 ± 13.7	82.1 ± 12.5	81.0 ± 14.1	0.195
Chest pain (cardiac vs. non-cardiac)	794/1324 (60.0 %)	274/334 (82.0 %)	520/990 (52.5 %)	0.685
Antiplatelet	801/1324 (60.5 %)	303/334 (90.7 %)	498/990 (50.3 %)	0.191
Statin	737/1324 (55.7 %)	286/334 (85.6 %)	451/990 (45.6 %)	0.914
Ace inhibitor	230/1324 (17.4 %)	96/334 (28.7 %)	134/990 (13.5 %)	0.567
Calcium blocker	125/1324 (9.4 %)	48/334 (14.4 %)	77/990 (7.8 %)	<0.05

Nitrates	335/1324 (25.3 %)	140/334 (41.9 %)	195/990 (19.7 %)	0.920
Betablocker	463/1324 (35.0 %)	216/334 (64.7 %)	247/990 (24.9 %)	0.180
Hyperlipidemia	802/1324 (60.6 %)	277/334 (82.9 %)	525/990 (53.0 %)	0.722

Table 2

Agatston score-derived features of obstructive and non-obstructive CAD groups (LM: left main, LAD: left anterior descending, LCX: left circumflex, and RCA: right coronary artery).

Features	Total (n = 1324)	Obstructive (n = 334)	Non-obstructive (n = 990)	p-value
LM Agatston Score	12.7 ± 52.1	36.0 ± 86.5	4.9 ± 29.5	<0.00001
LAD Agatston Score	118.0 ± 272.3	334.1 ± 434.3	45.1 ± 120.7	
LCX Agatston Score	52.7 ± 218.2	177.4 ± 399.5	10.6 ± 53.8	
RCA Agatston Score	100.2 ± 364.6	330.2 ± 657.9	22.6 ± 90.4	
Total Agatston Score	283.6 ± 724.0	877.7 ± 1210.3	83.1 ± 220.5	
Log (LM Agatston Score+1)	0.27 ± 0.63	0.65 ± 0.88	0.14 ± 0.45	
Log (LAD Agatston Score+1)	1.03 ± 1.08	2.10 ± 0.81	0.67 ± 0.90	
Log (LCX Agatston Score+1)	0.56 ± 0.89	1.44 ± 1.02	0.26 ± 0.59	
Log (RCA Agatston Score+1)	0.71 ± 1.00	1.70 ± 1.08	0.38 ± 0.72	

Log (total Agatston score+1)	1.28 ± 1.19	2.52 ± 0.77	0.86 ± 1.00	
Diffusivity index	0.15 ± 0.20	0.34 ± 0.19	0.09 ± 0.16	

Table 3

Classification results of each model obtained using 1000 repeated 5-fold cross validation. The exact same training and testing data were used for each model, with hyperparameter optimization using grid search.

Model	Sensitivity	Specificity	Accuracy	AUC
Model 1 (Clinical)	66.9 ± 5.7	87.2 ± 2.6	74.1 ± 3.1	77.9 ± 3.1
Model 2 (Clinical + AG-derived)	80.5 ± 9.8	92.8 ± 3.0	81.9 ± 1.3	90.0 ± 1.1
Model 3 (Clinical + AG-derived + Fat-omics)	83.5 ± 5.5	93.7 ± 1.9	82.4 ± 2.0	90.1 ± 0.9

Table 4

Comparison of the proposed method (CatBoost) against other established machine learning approaches, including random forest (RF), support vector machine (SVM), and XGBoost. Results were obtained using 1000 repeated five-fold cross validation. The exact same training and testing data were used for each method, with hyperparameter optimization using grid search.

Model	Sensitivity	Specificity	Accuracy	AUC
RF	72.6 ± 7.2	90.6 ± 2.2	84.9 ± 2.5	89.3 ± 3.1
SVM	92.2 ± 0.3	59.9 ± 1.1	76.0 ± 0.6	88.9 ± 0.2
XGBoost	74.0 ± 5.3	90.9 ± 2.1	84.1 ± 2.2	89.7 ± 2.4
CatBoost	83.5 ± 5.5	93.7 ± 1.9	82.4 ± 2.0	90.1 ± 0.9